*Materials Transactions*, Vol. 61, No. 11 (2020) pp. 2178 to 2184


# Development of VGCF/MP Reinforced Al Matrix Composite by Low Pressure Infiltration Method and Their Thermal Property

Fei Gao[1], Yongbum Choi[2,*] and Kazuhiro Matsugi[2]

[1]*Department of Mechanical Science and Engineering, Graduate School of Engineering, Hiroshima University, Hiroshima 739-8527, Japan*
[2]*Graduate School of Advanced Science and Engineering, Hiroshima University, Hiroshima 739-8527, Japan*

To fabricate vapor grown carbon fibers and mesophase pitch reinforced Al matrix (VGCF/MP/Al) composites, porous VGCF/MP with high porosity was fabricated using the spacer method. Carbonization and electroless Ni plating were carried out on porous VGCF/MP to improve its thermal conductivity (TC) and wettability with Al matrix, respectively. In addition, VGCF/MP/Al composites were manufactured using a low pressure infiltration method at 0.1 MPa. The effect of volume fraction of VGCFs on the interface between VGCF/MP and Al matrix, and the reactivity of the Al matrix to the Ni plating were investigated. The composites with 0.5 vol% of VGCFs showed a bonded interface between VGCF/MP and Al matrix. The bonded interface can be attributed to the improved wettability between VGCF/MP and Al matrix from Ni plating, resulting in the good bonding seen between VGCF/MP and Al matrix. At the interface of this sample, an intermetallic compound, $Al_3Ni$, formed from the reaction between Ni and Al. Furthermore, the thermal conductivities of the fabricated porous VGCF/MP and VGCF/MP/Al composites were determined. [doi:10.2320/matertrans.MT-M2020158]

(Received May 19, 2020; Accepted July 14, 2020; Published September 29, 2020)

***Keywords:*** *vapor grown carbon fibers, electroless plating, Al matrix composite, microstructure, thermal conductivity*

## 1. Introduction

The development of modern electronic devices requires heat sink materials with thermal conductivity (TC) of at least 200 $W \cdot m^{-1} \cdot K^{-1}$ and coefficients of thermal expansion (CTE) approximately 6–7 ppm/K.[1,2] Metal matrix composites (MMCs) with superior TC, CTE, and low density are promising candidates to replace traditional heat sink material in recent years.[3] Carbon fiber as reinforcement for MMCs are potential candidate because of their high thermal conductivity (TC) and ultra-low thermal expansion.[1–3] In particular, the TC of vapor-grown carbon fibers (VGCF), a kind of nano carbon fiber, is 1200 $W \cdot m^{-1} \cdot K^{-1}$,[4] which is higher than other carbon fibers (−800 $W \cdot m^{-1} \cdot K^{-1}$). It is also approximately 5 times higher than Al (237 $W \cdot m^{-1} \cdot K^{-1}$) and approximately 3 times higher than Cu (386 $W \cdot m^{-1} \cdot K^{-1}$).

As to the application in the electronic devices, plane fin heat sink is a common type of heat sink which functions to spread heat at the surface of fins. Based on Newton's law of cooling, materials with isotropy of heat direction are suitable to be used as plane fin heat sink material due to their efficient heat transfer at each surface of the plane fin.[5] To achieve MMC with isotropy, continuous phase reinforcement inside MMCs is necessary. However, carbon fibers have anisotropy. To solve this, a network structure of carbon fiber is necessary. In addition, the low pressure infiltration (LPI) fabrication method of MMCs with high volume fractions of reinforcements has gained traction in recent years.[6,7] In previous studies, VGCFs and mesophase pitch powder (MP) were sintered at 823 K to fabricate porous VGCF/MP as the preform with the network structure. The porous VGCF/MP was then utilized to fabricate MMCs with isotropy by LPI method.[8] However, VGCF, a kind of nanofiber, has the problem of aggerating and tangling together due to van der Waals forces and high aspect ratios. Moreover, the MP has a low TC after sintered at 823 K. These problems have a significant impact on the TC of fabricated MMCs. To achieve the TC of VGCF/MP reinforced Al matrix (VGCF/MP/Al) composites, the ideal porous VGCF/MP requires fewer micro-pores in the cell wall of the preform, good wettability with the Al matrix, and high TC.[6–8]

In this study, porous VGCF/MP were fabricated as the preform, and its microstructure and porosity were investigated. To improve the wettability of porous VGCF/MP with the Al matrix, electroless Ni plating was applied to the porous VGCF/MP. Moreover, carbonization at high temperature on the porous VGCF/MP improved the TC.[9] The effect of carbonization on the microstructure of MP was investigated. The VGCF/MP/Al composites were fabricated using the LPI process, and its microstructure and TC were examined.

## 2. Experimental

### 2.1 Raw materials and fabrication of the VGCF/MP/Al composites

VGCFs (density: 2.1 $kg/m^3$, Showa Denko Co., Japan, Fig. 1(a)), MP (density: 2.1 $kg/m^3$, JFE Chemical Co., Japan, Fig. 1(b)), and NaCl particles (density: 2.1 $kg/m^3$, size: 180–360 μm, Fig. 1(c)) were used to fabricate the porous VGCF/MP. The porous VGCF/MP were fabricated using the spacer method. First, the VGCFs, MP and NaCl particles were mechanically mixed (45° tilt) for 600 s using a glass rod. The NaCl particles were used as the spacer to obtain continuous pores in the porous VGCF/MP. To maintain constant infiltration conditions, the volume fraction of NaCl particles was fixed at 90 vol%. The resulting mixture was then placed in a graphite mold and compacted at a pressure of 60 MPa. Next, the compacted mixture was sintered in Ar. The sintering process was carried out at 823 K for 3.6 ks. Finally, the sintered samples were initially immersed in distilled water for 48 h to dissolve NaCl particles followed by drying. The

*Corresponding author, E-mail: ybchoi@hiroshima-u.ac.jp

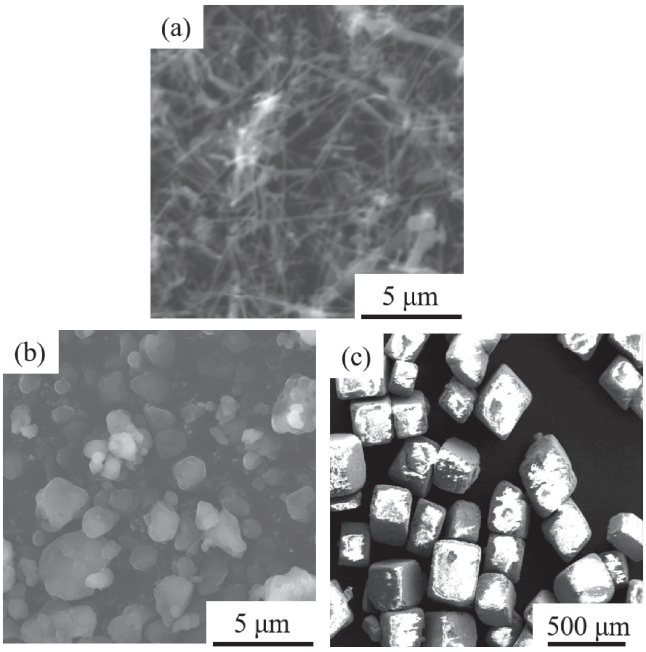


Fig. 1 SEM images showing the morphologies of (a) VGCFs, (b) MP powders, and (c) NaCl particles used in this study.

size of the porous VGCF/MP was $\phi 10 \times 10\,mm^3$. To obtain highly crystallized MP, carbonization was applied to porous VGCF/MP at 1773 K for 3.6 ks in Ar. Electroless Ni plating is a commonly used surface treatment method to improve wettability between Al and carbon materials and to prevent the formation of $Al_4C_3$.[10] Thus, electroless Ni plating was also applied on the porous VGCF/MP. The electroless Ni plating process involved the sensitization, activation, and plating steps.[11] The conditions required for electroless Ni plating process were pH 6.5 and temperature of 293 K for 300 s. Specifically, to obtain the plating layer at the surface of the cell wall in the porous VGCF/MP, the electroless Ni plating process was carried out in a vacuum box with a pressure of −0.8 MPa to fill the porous VGCF/MP with bathes at each step.

Table 1 Fabrication conditions of porous VGCF/MP.

| Sample | Volume fraction (vol.%) | | | Carbonization |
|---|---|---|---|---|
| | NaCl | MP | VGCFs | |
| 1 | 90 | 10 | 0 | Untreated |
| 2 | 90 | 10 | 0 | Treated |
| 3 | 90 | 9.5 | 0.5 | |
| 4 | 90 | 7 | 3 | |

Pure Al (purity ≥ 99.7%) was used as the matrix. A pure Al ingot and porous VGCF/MP were placed in a cylindrical graphite die and then heated to 1037 K in Ar. Subsequently, a pressure of 0.1 MPa was applied with a holding time of 3.6 ks to infiltrate molten Al into porous VGCF/MP. The schematic of the fabrication process for the VGCF/MP/Al composite is shown in Fig. 2 and the fabrication conditions of VGCF/MP/Al are shown in Table 1.

### 2.2 Characterization of microstructure, porosity, and thermal conductivity

The microstructure was examined using scanning electron microscope (SEM; JEOL, JXA-8900). To examine the effect of carbonization on MP, the MP were analyzed before and after carbonization using transmission electron microscope (TEM; JEOL, JEM-2010). X-ray diffraction (XRD; D/max-2500/PC, Japan) was also carried out using Cu K$\alpha$ radiation ($\lambda = 1.54056$ Å) at a scanning speed of 1°/min over the $2\theta$ range of 20°–90°. The elemental distribution of the composites was determined using electron probe micro-analyzer (EPMA, JXA8900-RL).

With the spacer method, the theoretical porosity is equal to the volume fraction of NaCl particles. However, porous VGCF/MP have micro-pores in its cell wall and closed pores. Thus, the effective porosity of porous VGCF/MP was calculated using the Archimedes method.[12] To calculate

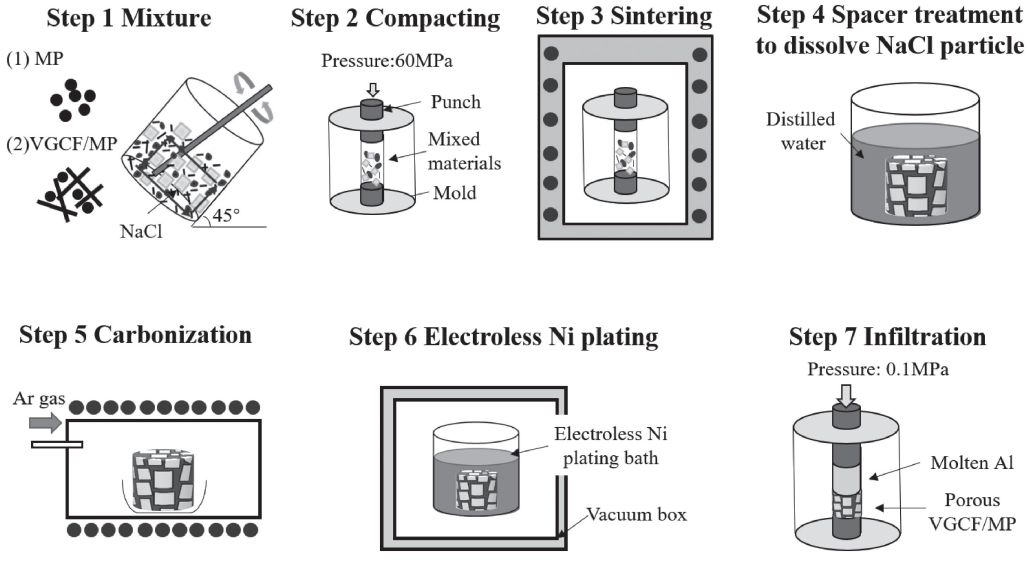


Fig. 2 Schematic of the fabrication process for preparing the VGCF/MP/Al composites.

the open porosity ($P_{open}$), total porosity ($P_{total}$), and closed porosity ($P_{closed}$), the following equations were used:

$$\rho_a = [W_1/(W_1 - W_2)] \times \rho_w \quad (1)$$

$$P_{open} = [(W_3 - W_1)/(W_3 - W_2)] \times 100 \quad (2)$$

$$P_{total} = (\rho_a/\rho_t) \times 100 \quad (3)$$

$$P_{closed} = P_{total} - P_{open} \quad (4)$$

where $W_1$, $W_2$ and $W_3$ refer to weight of dry preform, impregnated preform in the distilled water and impregnated preform, respectively; $\rho_a$, $\rho_t$, and $\rho_w$ refer to apparent density of preform, theoretical density of preform and density of distilled water (997.05 kg/m$^3$, 898 K), respectively. The TC of specimens ($\phi 10 \times 10$ mm$^3$) was characterized using the steady-state method.[13)]

## 3. Results and Discussions

### 3.1 Microstructure and porosity of the porous VGCF/MP

Figure 3 shows the SEM images of the porous VGCF/MP and its cell wall. As shown in Figs. 3(a)–(d), pores with size of 180–360 μm were formed by dissolved NaCl particles and continuous pores were formed by connected NaCl particles. Closed pores were also observed formed by isolated NaCl particles. In Figs. 3(a) and 3(b), the cell walls consisted of sintered MP. In Figs. 3(b) and 3(c), micro-pore with size of 1–2 μm was observed in the cell wall due to the removal of impurities by carbonization. In Figs. 3(c) and (d), the cell walls consisted of sintered MP and VGCFs. With the addition of VGCFs at 3 vol% however, numerous micro-pores with random shape and size ranging from 1–8 μm were observed in the cell wall, as shown in Fig. 3(d). This is due to the addition of VGCFs at 3 vol% resulting in the aggregation of VGCFs. Figure 4 illustrates the porosities of porous VGCF/MP using different fabrication conditions. In Fig. 4, the $P_{total}$ range of porous VGCF/MP was 91.0–91.9% while it was 95.1% for the porous VGCF/MP fabricated with 3 vol% VGCFs and after carbonization. The $P_{open}$ range of porous VGCF/MP was 87.9–88.72%, which indicated that the fabrication of porous VGCF/MP was achieved. The $P_{closed}$ range for porous VGCF/MP fabricated with the addition of 0–0.5 vol% VGCFs was 3.1–3.4%. The $P_{closed}$ variation is due to the closed pores in porous VGCF/MP corresponding with Figs. 3(a)–(c). However, with closed pores and micro-

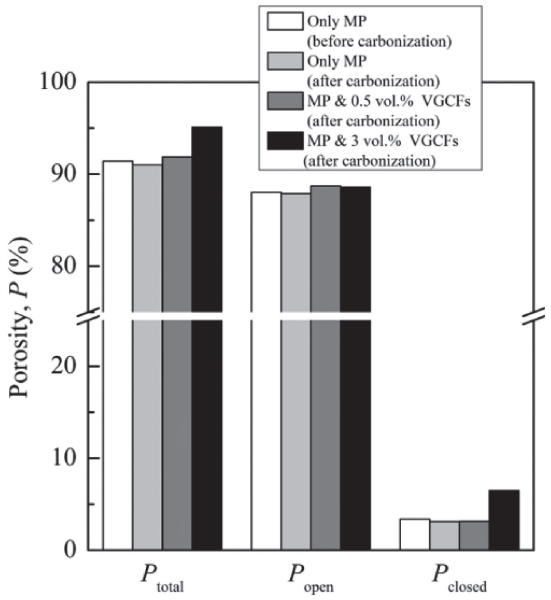


Fig. 4 Porosity of porous VGCF/MP under different fabrication conditions.

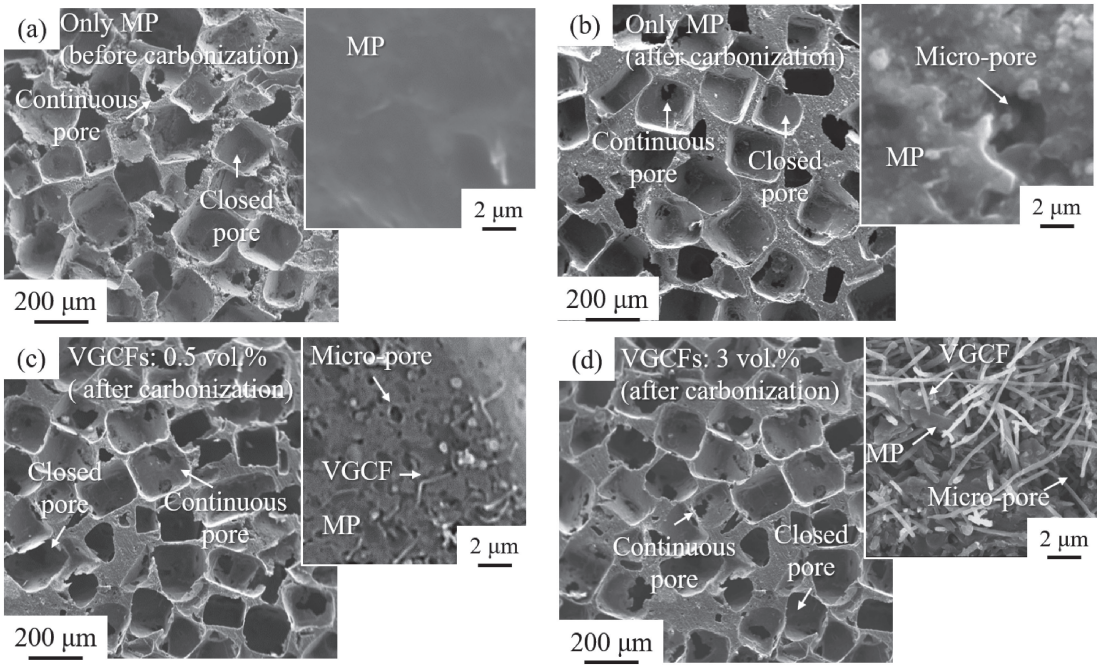


Fig. 3 SEM images of porous VGCF/MP: (a) only MP and before carbonization, (b) only MP and after carbonization, (c) MP & 0.5 vol% VGCFs and after carbonization, and (d) MP & 3 vol% VGCFs and after carbonization (the inserts are the inserts are magnified images of each porous VGCF/MP's cell wall).

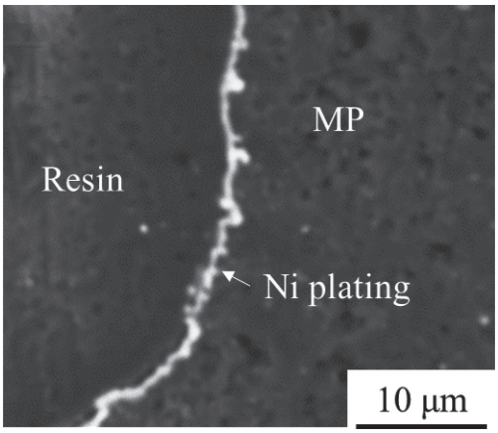


Fig. 5 BSE image of electroless Ni plated porous VGCF/MP (only MP and before carbonization) buried by resin.

pores in the cell wall of porous VGCF/MP after the addition of 3 vol% VGCFs (see Fig. 3(d)), the $P_{closed}$ was increased to 6.5%.

To examine the thickness of Ni plating applied on porous VGCF/MP, the Ni plated-porous VGCF/MP (only MP and before carbonization) were buried by resin and its BSE image is shown in Fig. 5. In Fig. 5, the resin filled the pore which formed by dissolved NaCl particle. The white region between resin and VGCF/MP represents the Ni plating. The thickness of Ni plating is approximately 1 μm.

Figure 6 shows the TEM images and XRD patterns of MP before and after carbonization. Comparing Figs. 6(a) and 6(b), the structure of MP was converted from a disordered structure to a layer structure by using carbonization. For FTT images in Figs. 6(a) and 6(b), halos became clear rings, indicating that MP were crystallized by carbonization.[9] In Fig. 6(c), the peak of the XRD pattern became especially sharp due to carbonization. This result proved that the MP had a high crystallinity from carbonization. Moreover, the full width at half maximum (FWHM) of (002) deceased from 5.280° to 1.528°. The decrease in FWHM of (002) indicated that the distance between carbon aggerates decreased,[14] resulting in higher phonon velocity in the porous VGCF/MP.[15]

### 3.2 Microstructure of the VGCF/MP/Al composites

Figures 7(a)–(d) shows the microstructures of the VGCF/MP/Al fabricated under different conditions. The dark and gray regions represent the VGCF/MP and the Al matrix, respectively. In Figs. 7(a)–(d), the VGCF/MP is a continuous phase in the Al matrix. This result indicated that the fabrication of VGCF/MP/Al composites with anisotropy was achieved. However, there were voids observed in Figs. 7(a)–(d). As shown in the magnified SEM images in Fig. 7(a), the void was surrounded by VGCF/MP and had the same shape as the closed pore in Fig. 3. The reason was that the closed pores were isolated from other pores in porous VGCF/MP. The molten Al did not infiltrate this part of the VGCF/MP/Al composites in LPI processing. Moreover, the interface between VGCF/MP and Al matrix, which was affected by the volume fraction of VGCFs, has a significant

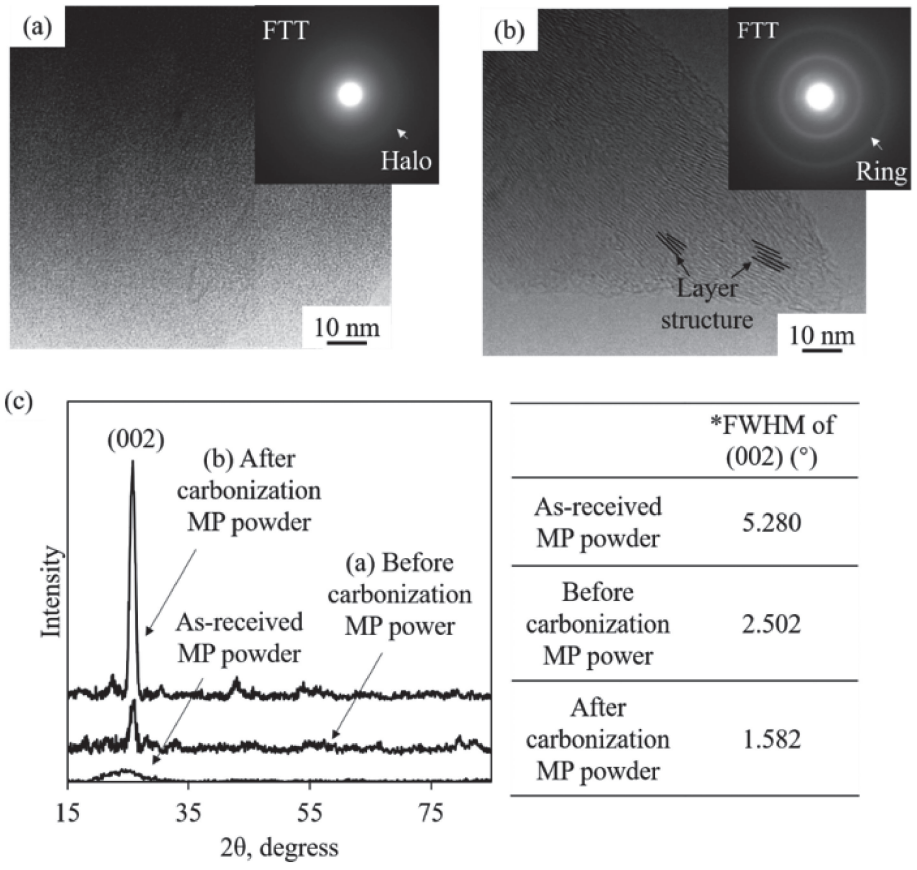


| | *FWHM of (002) (°) |
|---|---|
| As-received MP powder | 5.280 |
| Before carbonization MP power | 2.502 |
| After carbonization MP powder | 1.582 |

Fig. 6 TEM images of MP insert with FTT: (a) before carbonization, (b) after carbonization, and (c) XRD patterns of as-received, before and after carbonization MP, and *FWHM of (002) corresponding pattern. (*FWHM: full width at half maximum)

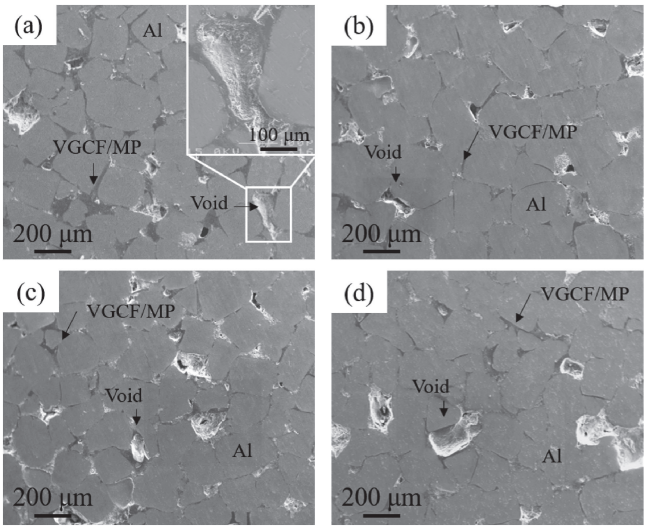


Fig. 7 SEM images of VGCF/MP/Al composites: (a) with only MP and before carbonization, (b) with only MP and after carbonization, (c) with MP & 0.5 vol% VGCFs and after carbonization, and (d) with MP & 3 vol% VGCFs and after carbonization.

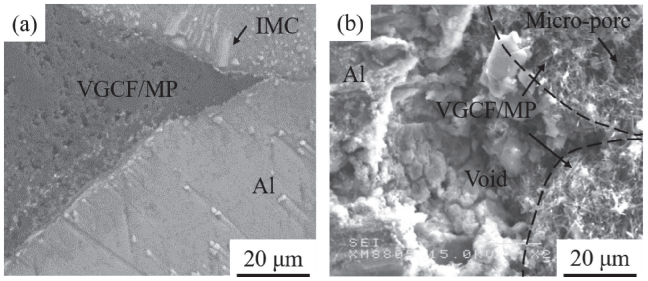


Fig. 8 SEM images of interface between VGCF/MP and Al matrix: (a) with MP & 0.5 vol% VGCFs and after carbonization, and (b) with MP & 3 vol% VGCFs and after carbonization.

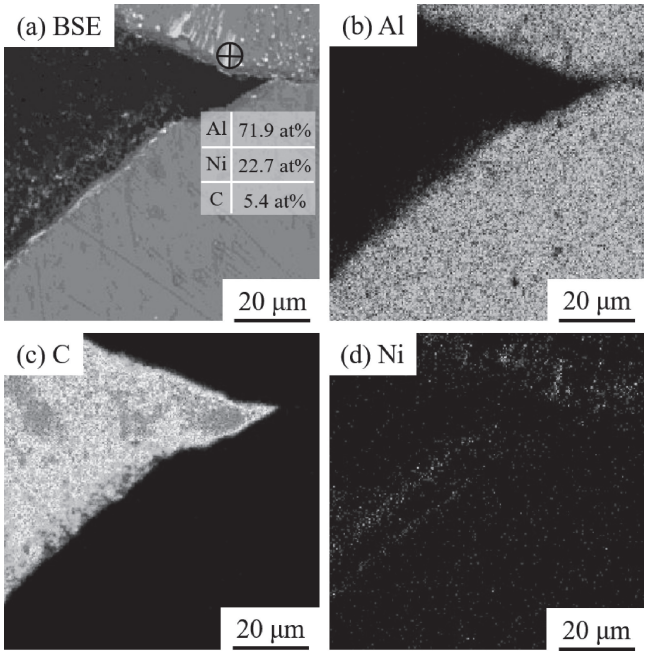


Fig. 9 Element distribution of VGCF/MP/Al composites fabricated under condition of MP & 0.5 vol% VGCFs and after carbonization: (a) BSE image (inset for location and result of point analysis), (b) Al element, (c) C element, and (d) Ni element.

impact on the TC of fabricated VGCF/MP/Al composites. Thus, the interfaces between VGCF/MP and Al matrix with addition of 0.5 and 3 vol% were observed, and the results are shown in Figs. 8(a) and 8(b), respectively. In Fig. 8(a) showing the VGCF/MP/Al composite with addition of 0.5 vol% VGCFs, the interface between the VGCF/MP and Al matrix is bonded. The bonded interface can be attributed to the improved wettability between VGCF/MP and Al matrix from Ni plating. A light-gray phase was observed in the Al matrix. This can be inferred to be metallic compounds (IMCs) formed by the reaction of the Ni plating and molten Al. In Fig. 8(b) showing the VGCF/MP/Al composite with addition of 3 vol% VGCFs, a void was observed at the interface between VGCF/MP and Al matrix. A gap at the side of VGCF/MP was also observed. Due to the addition of 3 vol% VGCFs, the VGCF/MP aggerated, resulting in the VGCF/MP becoming discontinuous rather than a continuous structure (see Fig. 8(a)). Moreover, the Ni plating was not observed at the side of the VGCF/MP. This indicates that the gap caused by the aggregation of VGCF/MP hindered the formation of Ni plating. Specifically, the gap had an acute angle, causing the bathes utilized in the electroless Ni plating process being unable to infiltrate this part. Due to poor wettability and the lack of Ni plating between Al and carbon materials, the void at the interface between VGCF/MP and Al matrix was formed.

To investigate the elemental distribution of VGCF/MP/Al composite (MP and 0.5 vol% VGCFs, after carbonization), EPMA was carried out in the same area as Fig. 8(a). The result is shown in Fig. 9. Furthermore, point analysis of IMC was carried out on the region marked with a cross in Fig. 9(a). The Al:Ni atomic ratio in the IMC region was found to be approximately 3:1. In Figs. 9(b) and 9(d), the Al and Ni overlapped in the IMC regions, indicating the formation of Al–Ni IMCs. Specifically, the IMC was identified to be $Al_3Ni$. The reaction at the interface between VGCF/MP and Al matrix was shown in eq. (5):

$$3Al + Ni = Al_3Ni \quad (5)$$

Moreover, there was no overlapping region between the Al element and the C element (see Figs. 9(b) and 9(c)). This indicates that Ni plating prevented the reaction between the molten Al and VGCF/MP. Therefore, there was no formation of $Al_4C_3$ at the infiltrating temperature of 1037 K.

### 3.3 TC of porous VGCF/MP and VGCF/MP/Al composite

The TC of fabricated porous VGCF/MP and VGCF/MP/Al composite under different fabricated conditions are shown in Figs. 10(a) and 10(b), respectively. In Fig. 10(a), the TC of porous VGCF/MP increased due to the crystallization of MP and addition of 0.5 vol% VGCFs. As heat in nonmetal is transferred by phonon, the MP with higher crystallization had a higher phonon velocity compared to MP before carbonization.[16] The VGCF was found to have a TC of 1200 $W \cdot m^{-1} \cdot K^{-1}$. Therefore, the TC of porous VGCF/MP improved due to the carbonization and addition of 0.5 vol% VGCFs. However, as the volume fraction of VGCFs

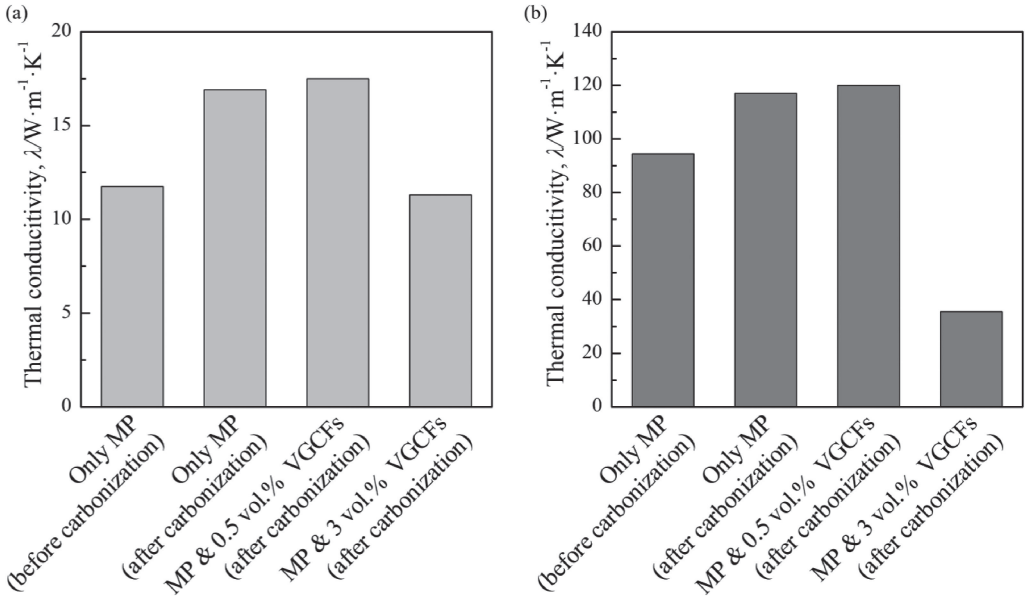


Fig. 10 TC of (a) porous VGCF/MP and (b) VGCF/MP/Al composites under different fabrication conditions.

increased to 3 vol%, the TC of porous VGCF/MP decreased. The porosity has a significant impact on the TC of the porous materials.[17] The decrease in the TC can be attributed to micro-pores resulting from the aggregation of VGCF/MP in the cell wall. In Fig. 10(b), the TC of the VGCF/MP/Al composite is consistent with the TC of porous VGCF/MP (see Fig. 10(a)). Moreover, as the addition of VGCFs increased from 0.5 to 3 vol%, the TC of the VGCF/MP/Al composites decreased significantly from 120.1 $W \cdot m^{-1} \cdot K^{-1}$ to 35.5 $W \cdot m^{-1} \cdot K^{-1}$. This is because at the 3 vol% VGCFs, the micro-pores in cell wall was not able to be infiltrated, and the voids at the interface between VGCF/MP and Al matrix. However, the TC of these composites with 0.5 vol% VGCF and carbonization were lower than the TC of Al (237 $W \cdot m^{-1} \cdot K^{-1}$). This is due to the thermal resistance at the interface[18] and the formation of $Al_3Ni$ which has a TC of approximately 35 $W \cdot m^{-1} \cdot K^{-1}$.[19] In the Al–Ni system, the formation of $Al_3Ni$ can be suppressed by adding Ni to the Al matrix. Also, to improve on this study, a higher crystallized MP can be achieved by utilizing temperature higher than 1037 K.[9,20] This will improve the TC of VGCF/MP/Al composites. It has also been reported that the carbon nanofiber reinforced Al matrix composites with TC over 200 $W \cdot m^{-1} \cdot K^{-1}$ can be fabricated via powder metallurgy.[21] However, unlike the powder metallurgy method, a low infiltration pressure of 0.1 MPa was utilized in this paper for the fabrication of the VGCF/MP/Al composites. The low pressure infiltration method allows for the fabrication of composites necessary for heat sinks with a large size and complex shape.[22] The data presented in this study does indicate the viability of these composites for industrial use and the commercialization of the final product. Thus, while still needing further study, VGCF/MP/Al composites, are potential materials for heatsinks in the future.

## 4. Conclusions

The porous VGCF/MP with high porosities were prepared using the spacer method. The VGCF/MP/Al composites were successfully fabricated using the LPI method at 0.1 MPa. The main conclusions of the study are presented here.

(1) In the porous VGCF/MP, pores with size of 180–360 μm were formed in dissolved NaCl particles. The cell walls of porous VGCF/MP were sintered with MP. With volume fraction ranging from 0 to 0.5 vol%, the cell walls of porous VGCF/MP had a continuous structure. With the addition of VGCF at 3 vol% however, numerous micro-pores formed due to the aggregation of VGCFs in the cell wall. This resulted in the $P_{closed}$ increasing to 6.5%. With carbonization, the structure of MP converted from a disordered structure to a layered structure; the MP also had a high crystallinity.

(2) VGCF/MP/Al composites with anisotropy were achieved by utilizing the VGCF/MP as a continuous phase in the Al matrix. However, the voids with the same shape as NaCl particles were observed in the VGCF/MP/Al composites for the closed pores. The VGCF/MP/Al composites with the addition of 0–0.5 vol% VGCFs had a bonded interface between VGCF/MP and Al matrix. With the addition of 3 vol% VGCFs however, a void was formed due to the aggregation of VGCF/MP. The Ni plating improved the wettability between VGCF/MP, and $Al_3Ni$ was formed from the reaction between the Ni plating and Al matrix in infiltration process.

(3) With carbonization and the addition of 0.5 vol% VGCFs, the TC of the VGCF/MP/Al composites increased because of the crystallization of the MP and the high TC of the VGCF. However, with the addition of 0.5 vol% VGCFs, the TC of the VGCF/MP/Al composite decreased due to the aggregation of VGCFs. The $Al_3Ni$ in Al matrix was detrimental to the TC of VGCF/MP/Al composites.

## REFERENCES


1) P.K. Schelling, L. Shi and K.E. Goodson: Mater. Today **8** (2005) 30–35.
2) S. Mallik, N. Ekere, C. Best and R. Bhatti: Appl. Therm. Eng. **31** (2011) 355–362.
3) G. Lalet, H. Kurita, J.M. Heintz, G. Lacombe, A. Kawasaki and J.F. Silvain: J. Mater. Sci. **49** (2014) 397–402.
4) Y.-M. Chen and J.-M. Ting: Carbon **40** (2002) 359–362.
5) B.L. Whatley: U.S. Patents, 2005.
6) S. Ren, X. He, X. Qu and Y. Li: J. Alloy. Compd. **455** (2008) 424–431.
7) B.S. Rao and V. Jayaram: Acta Mater. **49** (2001) 2373–2385.
8) F. Gao, Y. Choi, K. Matsugi, Z. Xu, K. Sugio and G. Sasaki: 21st International Conference on Composite Materials, (Chinese Society for Composite Materials, Xi'an, 2017).
9) Y. Arai: Nippon Steel Technical Report. **59** (1993).
10) S. Ip, R. Sridhar, J. Toguri, T. Stephenson and A. Warner: Mater. Sci. Eng. A **244** (1998) 31–38.
11) Y. Choi, Z. Zu, K. Matsugi, K. Sugio and G. Sasaki: Mater. Trans. **58** (2017) 834–837.
12) J. Locs, V. Zalite, L. Berzina-Cimdina and M. Sokolova: J. Eur. Ceram. Soc. **33** (2013) 3437–3443.
13) F.R. Feret: Analyst **123** (1998) 595–600.
14) M. Lee, Y. Choi, K. Sugio, K. Matsugi and G. Sasaki: Mater. Trans. **52** (2011) 939–942.
15) S. Bourdo, Z. Li, A.S. Biris, F. Watanabe, T. Viswanathan and I. Pavel: Adv. Funct. Mater. **18** (2008) 432–440.
16) S.I. Oh, J.Y. Lim, Y.C. Kim, J. Yoon, G.H. Kim, J. Lee, Y.M. Sung and J.H. Han: J. Alloy. Compd. **542** (2012) 111–117.
17) J.W. Paek, B.H. Kang, S.Y. Kim and J.M. Hyun: Int. J. Thermophys. **21** (2000) 453–464.
18) K. Sugio, Y. Choi and G. Sasaki: Mater. Trans. **57** (2016) 582–589.
19) Y. Terada, K. Ohkubo, T. Mohri and T. Suzuki: Mater. Trans. **43** (2002) 3167–3176.
20) V. Gergely and B. Clyne: Adv. Eng. Mater. **2** (2000) 175–178.
21) F. Ogawa, S. Yamamoto and C. Masuda: Acta Metall. Sin. (Engl. Lett.) **32** (2019) 573–584.
22) J. Kaczmar, K. Pietrzak and W. Włosiński: J. Mater. Process. Technol. **106** (2000) 58–67.